By Gerrit Adriaan Folkertsma, Wessel Straatman, Nico Nijenhuis, Cornelis Henricus Venner, and Stefano Stramigioli

Robird

A Robotic Bird of Prey

Ever since the start of aviation, birds and airplanes have posed a mutual risk: Birds are killed when struck by aircraft, but, in return, bird strikes cause billions in damage to the aviation industry. Airports employ bird-control methods such as audiovisual deterrents (like scarecrows, lasers, and noise), weapons, and chemicals to relocate, suffocate, or otherwise terminate the birds [2]. While the latter methods work, they are ethically questionable. The problem of audiovisual deterrents is that they quickly lose effectiveness due to habituation. The approach that works consistently is the use of predator birds to scare off the prey birds and permanently relocate them away from runways. However, the predators themselves cannot be precisely controlled and, in turn, also pose a threat to airplanes.

The Robird is a robotic bird mimicking a peregrine falcon in appearance, weight (730 g), size (112-cm wingspan), and flying speed (16 m/s). Most importantly, the Robird is a flapping-wing aerial vehicle, mimicking the method of flight of a real falcon. The similarity in appearance and dynamics means that other birds cannot distinguish real falcons from the Robird. This allows the Robird to be used for effective and nature-friendly bird control. From a research perspective, the Robird is most interesting. Much is still unknown about how the Robird flies. The challenges lie in understanding its aerodynamics and improving its autonomy.

Digital Object Identifier 10.1109/MRA.2016.2636368
Date of publication: 7 June 2017

1070-9932/17©2017IEEE

The Need for Robirds

Homo universalis Leonardo da Vinci dreamed of bird-like flying machines in his "Codex on the Flight of Birds" [1]. Failing to make those work, we have since switched to fixed-wing aircraft that perform admirably well—until they come into contact with an actual bird. Worldwide, bird strikes lead to annual damages in the billions of dollars, with a risk of plane crashes.

The danger that aviation poses to birds, and, in turn, to itself, necessitates the relocation of birds around airports. Conventional bird-control methods lose their effectiveness due to habituation, and more violent, ethically questionable approaches meet resistance from environmental agencies and the public in general. The use of birds of prey, such as falcons or eagles, is a very effective natural approach since the fear of these natural enemies is bred into the birds that require relocating; additionally, the approach does not lose effectiveness [2]. Aside from the collision risk that the birds of prey themselves pose, these birds need to rest frequently and are by nature nocturnal, which limits their availability.

Fixed-wing or quadrotor remotely piloted aircraft systems (RPAS) have the short-term effectiveness of scattering birds, but they also suffer from habituation. Better results have been obtained with fixed-wing RPAS that look like predator birds, although actual birds of prey are not fixed-wing: they use flapping flight when hunting, so results may be improved by using an ornithopter capable of flapping and soaring [3], [4].

Robirds are robotic birds that closely resemble natural birds, both in appearance and in flight behavior: They fly by flapping their wings, can soar, and have speed and wing frequencies similar to a real bird. The peregrine falcon model can fly up to 60 km/h (16 m/s) and has the same effect on prey birds as a real peregrine falcon. Its only downtime is the changing of batteries, and it can be controlled to stay off the runways. It is a perfect nature-inspired and nature-friendly means of bird control for aviation safety.

Research Perspective

The first peregrine falcon Robird was painstakingly put together by a falconer and model airplane enthusiast in a backyard shed [5]. Through his experience with model airplanes and the study of his birds, he managed to make a working prototype by trial and error. Usually, in engineering research, we design a device that, theoretically, should work, and subsequently spend much time and effort trying to make it work. Here, it is the opposite: we have a working system, but no real insight yet into how it works!

The Robird offers myriad research opportunities. How does it fly? What is the unique combination of dynamics and aerodynamics that leads to its high-performing flight? Once we can understand these things, we can tackle the engineering challenge of improving the design so that it can fly on autopilot, run longer on a single battery charge, become self-stabilizing, and so forth. We can also use the Robird to study nature: How do prey birds react to the robotic counterpart of their natural enemy? Will studying the Robird's flight lead to insight into real bird flight?

Other Ornithopters

There is a range of flapping-wing vehicles, or ornithopters, differing in scale and similarity to the animals they are modeled after. Festo's SmartBird was inspired by a gull, and it very closely mimics the wing kinematics of a real gull [6]. It achieves a graceful flight with fully actuated wings; however, its size is far greater than its biological counterpart and its weight is less, resulting in much slower flight dynamics. The bird can only fly in very light wind conditions. A bioinspired ornithopter that focuses more on dynamic similarities in flight behavior is the DelFly, an insect-like flapping-wing micro-aerial vehicle that can both hover and fly up to 7 m/s [7]. A single spar drives its wings, relying on the wing's flexibility for proper wing motion. Similarly, but on a different scale, Harvard's Robobee mimics the flight of a bee. It has the same size, achieving dynamics and aerodynamics comparable to the honeybee [8]. Also driven by a single spar, its shoulder has a passive hinge for tilting the wings.

Birds are killed when struck by aircraft, but, in return, bird strikes cause billions in damage to the aviation industry.

Like the Robobee, the Robird is matching dynamics and aerodynamics to its biological inspiration to achieve similar performance. It combines two spars with proper wing flexibility to achieve the required flapping motion. The Robird is the first ornithopter to do this in the weight and speed range of predator birds.

The Peregrine Falcon and the Bald Eagle

There are currently two Robird models, the peregrine falcon and the bald eagle (Figure 1). They can reach speeds of 60 and 90 km/h (16 and 24 m/s), respectively, and fly in wind speeds of up to 6 Beaufort (13 m/s). They stay airborne by a combination of wing and body shape, active wing pitch control, wing flexibility, and various control surfaces for stabilization. Visit https://vimeo.com/robirds to see several videos of the bird in flight.

While the bald eagle model flies faster and can carry a payload of up to 1 kg, it is, due to its size and weight, also slightly more unwieldy than the peregrine falcon. More importantly, the birds we are targeting at airports are preyed upon by the falcon. Therefore, our research in this article focuses on the peregrine falcon model. In the remainder of this article, we will refer to the peregrine falcon model simply as the Robird. Table 1 shows some physical characteristics of the two models and a comparison to the real birds.

Figure 1. (a) A peregrine falcon. (Photo courtesy of Julien Baudat-Franceschi.) (b) The Robird peregrine falcon model and (c) the bald eagle model.

Table 1. Physical characteristics of the bald eagle, peregrine falcon, and their robotic counterparts [9].

	Bald Eagle		Peregrine Falcon	
	Bird	**Robird**	**Bird**	**Robird**
Mass	3.0–6.3 kg	2.1 kg	0.6–1.3 kg	0.73 kg
Body length	70–102 cm	88 cm	39–50 cm	56 cm
Wingspan	1.8–2.3 m	1.76 m	0.95–1.15 m	1.12 m
Flight speed	15–20 m/s	18 m/s	18–25 m/s	16 m/s

System

The key feature of the Robird is its flapping-wing flight. Both thrust and lift are produced by a combination of the shape and flexibility of the wings and the mechanism that not only flaps the wings (a plunging motion), but also changes their angle of attack (pitching) during the wing stroke. The wings and tail have control surfaces for stabilization; the mechanism (Figure 2) and avionics for the autopilot reside inside the hull (Figure 3).

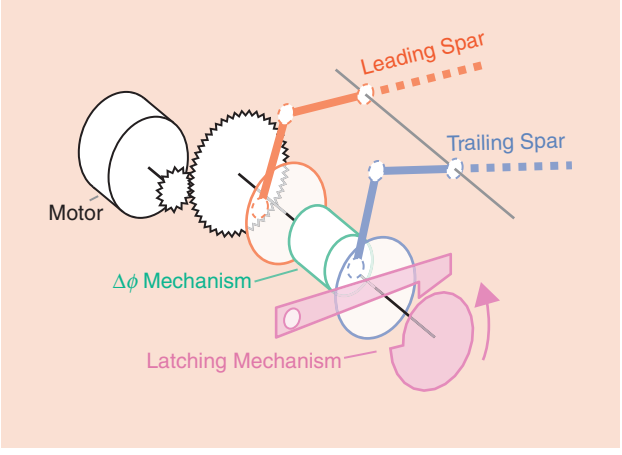

Figure 2. A schematic drawing of the wing mechanism. The leading and trailing edge of the wing are driven with a phase difference of $\Delta\phi \in [0°,15°]$. Their rotation is transformed to a flapping motion of the wing through a connection rod mechanism for each driving spar. If the motor is stopped at the right time, lift pressure pushes the notch wheel against the pawl (latching mechanism), which allows the Robird to soar with the motor turned off.

Wings and Mechanism

The plunging and pitching motion of the wings is realized by driving them up and down at the leading and trailing edge of the wing, with the leading edge also leading by a small phase difference $\Delta\phi \in [0°, 15°]$. Figure 2 gives a schematic overview of the mechanism. It has a latch to lock the wings in a gliding position, allowing the Robird to soar with the motor turned off. This glide mode operation is explained more fully in the "Flight Modes" section.

The wings are made of foam with a laminated resin skin, resulting in a lightweight and flexible material. While the two spars that drive the wing introduce some pitching, the flexibility combined with aerodynamic forces causes additional twisting, leading to a more favorable angle of attack toward the distal end of the wing. The shape, especially the sharp transition from straight to swept wing and possibly the jagged trailing edge, have turned out to be crucial for generating and subsequently shedding vortices that generate thrust and lift (Figure 4).

Control Surfaces

The Robird has three control surfaces: a spoiler on each wing (see Figure 4) and an elevator in the tail. The hinge and attachment point of the latter are just discernible in Figure 3. While the elevator functions as a direct pitch control, steering with spoilers is rather complicated: When opened, they cause reduction of lift at that wing and induce a roll motion. At the same time, their drag induces a yawing motion. Whereas the yawing initially helps to start a turn, once the Robird is rolled on its side, the same motion pitches the nose downward, which leads to a loss of altitude.

The latest version of the Robird incorporates a V-shaped tail with two control surfaces that act as a combined rudder and elevator. Preliminary tests show that stability and flight performance is increased, though at the cost of a slight deviation from the real bird's appearance.

Avionics

The bird is driven by a brushless dc motor (maximum 112-W output at 11.1 V) and powered by a regular, hobby-grade electronic speed controller (ESC). The control surfaces are actuated using standard remote control (RC) servos. All actuators are controlled by an ArduPilot Mega/Pixhawk autopilot system running on a PX4 embedded computing board [10]. The redundant and fail-safe design of the software and hardware is indispensable when flying on or near airports.

Robustness

Limited robustness is a well-known problem in ornithopters. Because of the violent wing motions, there is much strain on the mechanics. However, the mechanism consists of just two connection rod mechanisms, and the wings consist of reinforced foam with no further actuators in the new V-tail model. Due to the relative simplicity of this system, the Robirds typically have a mean time between failures of several flight hours, which equals many 10–15-min flights.

Dynamic System Model

Studying the dynamics of the Robird to learn how it flies is interesting. Moreover, detailed understanding is a prerequisite for improvements to and optimization of the system. State estimation, controller (autopilot) design, and drivetrain optimization all benefit from better knowledge of the bird's dynamics.

Fixed-Wing Aerodynamics

In fixed-wing flight mode, the aerodynamics of the Robird are essentially equal to those of a glider. A glider's performance can be expressed by its glide number, the maximum lift/drag ratio [11]

$$(L/D)_{\max} = \frac{1}{2}\sqrt{\frac{\pi e AR}{c_{D,0}}}, \tag{1}$$

where AR is the glider's aspect ratio, b^2/S, where b is the total wingspan and S the wing area plus the area of the body directly between the wings; $c_{D,0}$ is the drag coefficient at zero lift ($c_L = 0$); and e is the Oswald span efficiency factor [12], [13].

The values for the Robird model (see Table 2) give a glide ratio of 8.3. This implies that it can cover a forward distance of 8.3 m for every 1-m loss in altitude. For comparison, the glide ratio for a glider plane is over 40, and that of a Boeing 747 is approximately 14. There is some discrepancy between this theory and experiments with a Robird scale model, where a glide ratio of up to 18 was observed for very high Reynolds numbers. It is still unclear what causes this discrepancy, but the real falcon has a similar low-glide ratio of 10 [14]. The Robird's poor performance as a glider is partly due to the locking mechanism, which locks the wings when moving downward with a negative angle of attack. Also, the drag coefficient $C_{D,0}$ is very high—the wing shape of both a

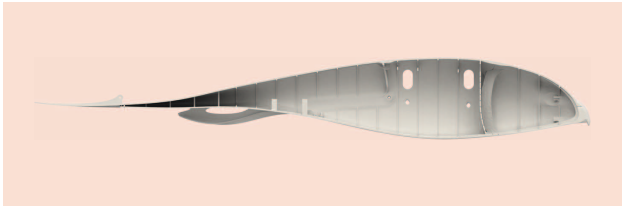

Figure 3. The hull of the Robird.

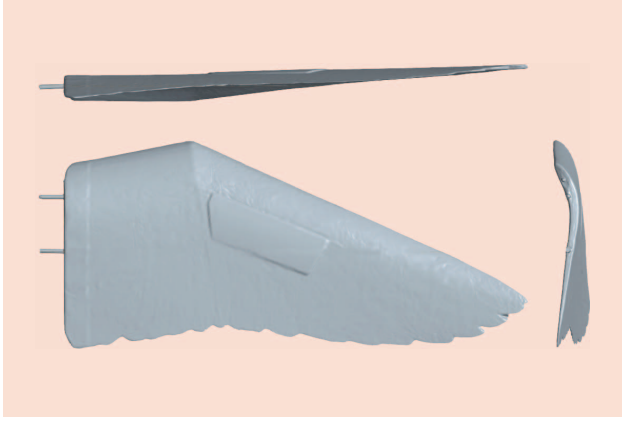

Figure 4. The wing of the Robird. Note the spoiler—the trapezoidal patch in the center—used for rolling maneuvers and the two spars used for driving the wing.

Table 2. Aerodynamic parameters for the glide ratio calculation of the Robird.

Parameter	Value	Description
$C_{D,0}$	0.08	Drag Coefficient $c_L = 0$
e	0.81	Oswald Span Efficiency Factor
b	1.12	Wingspan, m
S	0.145	Wing Surface Area [m^2]

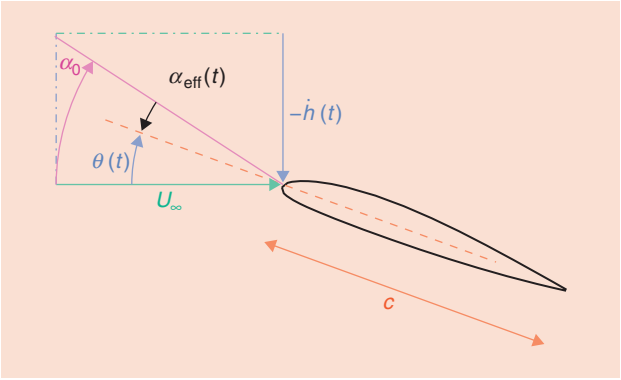

Figure 5. A 2-D cross-section of the wing: The plunging velocity $(\dot{h}(t))$ and flight velocity U_∞ result in an angle-of-attack α_0, which is reduced due to pitching $(\theta(t))$ to the effective angle-of-attack $\alpha_{\text{eff}}(t)$. (The chord length of the wing is c.)

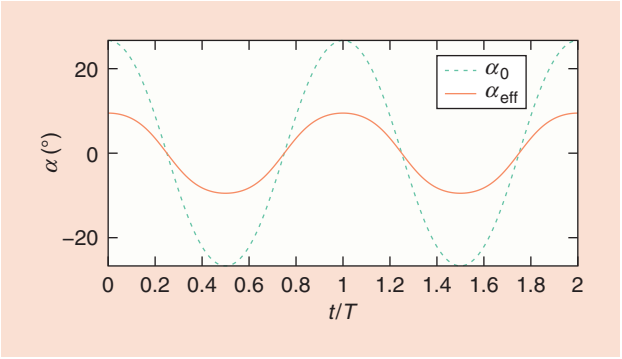

Figure 6. The effective angle of attack α_{eff} is a result of the interplay of the plunging motion $(\dot{h}(t))$ with the free-stream (flight) velocity U_∞ and the wing's active pitching. Without pitching, the wing would stall because of the high angle of attack (α_0).

falcon and Robird is clearly optimized for fast flapping-wing flight.

Flapping-Wing Aerodynamics

Much more interesting and challenging to characterize is the flapping-wing flight regime. There are no precise analytical results to calculate lift and thrust generation, and even numerical methods can only give an approximation [15]. Qualitatively, however, flapping-wing flight works as shown in the following sections.

Kinematics

A two-dimensional (2-D) cross-section of the wing (Figure 5) moves as follows:

$$\begin{cases} h(t) = h_0 \sin(\omega t) \\ \theta(t) = \theta_0 \sin(\omega t + \varphi), \end{cases} \tag{2}$$

where h_0 and θ_0 are amplitudes of the plunging and pitching motion and φ is the phase difference between the plunging and pitching motion determined by the phase offset between the two driving spars, as shown in Figure 2. From these kinematics, the effective angle of attack α_{eff} can be found

$$\alpha_{\text{eff}}(t) = \arctan\left(\frac{-\dot{h}(t)}{U_\infty}\right) + \theta(t). \tag{3}$$

For the midwing cross-section of the Robird, $\theta_0 = 17.12°$ and $h_0 = 16$ cm. For a flight velocity of 14 m/s, α_{eff} is shown in Figure 6. The active pitching of the wing reduces the effective angle of attack, which is vital for stable flight.

Characteristic Dimensionless Numbers

In flapping-wing flight, the Strouhal number is an essential characteristic dimensionless number [16]. It can be calculated by

$$\text{St} := \frac{kh_0}{\pi c}, \tag{4}$$

where c is the average chord length of the wing, k is reduced flapping frequency, nondimensionalized with c and flight speed U_∞, as in [17]

$$k := \frac{\omega c}{U_\infty}. \tag{5}$$

Taylor et al. [16] have shown that the Strouhal number lies between 0.2 and 0.4 in cruising flight for 42 different species of flying animals as well as sharks, fish, and dolphins. For the Robird, it lies just below 0.4.

The effective angle of attack α_{eff} depends directly on the Strouhal number, as shown in (6). If α_{eff} is in the proper range, the wing is always on the onset of dynamic stall: A leading-edge vortex (LEV) is generated along the leading edge of the wing, travels in chordwise direction, and is finally shed into the wake at the trailing edge. These LEVs are essential for flapping-wing flight

$$\begin{aligned} \alpha_{\text{eff}}(t) &= \arctan\left(\frac{-\dot{h}(t)}{U_\infty}\right) + \theta(t) \\ &= \arctan\left(\mathbf{St}\, \pi \cos(\omega t)\right) + \theta(t). \end{aligned} \tag{6}$$

Von Kármán Vortex Street

In an airflow, vortices are generated and shed around stationary blunt objects, resulting in a so-called Von Kármán vortex street—a series of vortices that are shed, alternating on the two sides of the object, rotating clockwise above and counterclockwise below the object. The vortex street induces a velocity field at the object, resulting in an oscillating force on the object that can cause it to vibrate (e.g., conductor gallop in power lines). In its wake, the vortex street induces a deficit in the streamwise velocity that is reminiscent of the object experiencing a drag force.

In bird flight, the plunging and pitching causes the vortices to be shed such that the top and bottom vortices are switched, and a reversed Von Kármán street is generated. The vortex street now causes a rearward-pointing jet-like flow that induces a thrust force on the wing.

Dynamics

All of the aerodynamics results presented in the preceding section start from an observation of the wing motion, which is then used as a rigid (kinematic) input to a computational fluid dynamics (CFD) method. To truly understand the flight behavior, the full fluid-structure interaction should be solved. In reality, the wing is not a rigid input to the airflow; rather, there is an interconnection, a bidirectional interaction, between fluid dynamics and structural dynamics.

While in theory it is possible to generate a fine finite element method model of the wing and connect it to a CFD model of the surrounding air—numerically solving the Navier–Stokes equations in conjunction with wing deformation—this would require enormous computation resources. The solution of this problem lies in proper simplification.

Currently, we are working on dividing the wing in a number of rigid bodies in port-Hamiltonian systems form, which gives them a power port for interacting with the aerodynamics. The optimal number and distribution of bodies and their parameters (mass, coupling stiffness, and damping) are determined by comparing simulations with experiments in a wind tunnel. We place markers on the wing (visible in Figure 7) and, with a stereoscopic camera setup and a stroboscope, obtain high-frequency three-dimensional (3-D) wing motion at various wind speeds, flapping frequencies, and leading-trailing edge phase differences. The port-Hamiltonian lumped-system model is then numerically optimized to show the same motion.

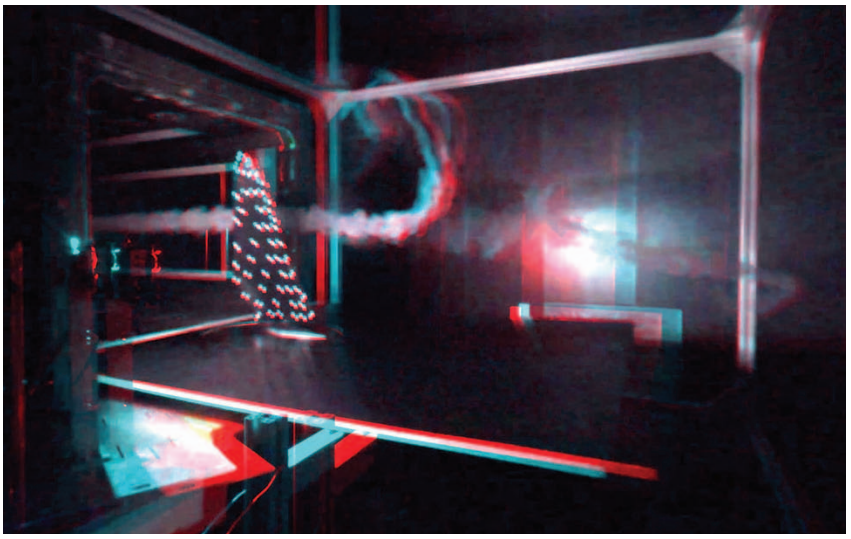

Figure 7. 3-D smoke trail measurements in the wind tunnel. Use a pair of red/cyan anaglyphic glasses to see the 3-D effect. The inlet of the tunnel is on the left, with the wing positioned right in front of it. The smoke trail shows the vortex street that is generated by the wing.

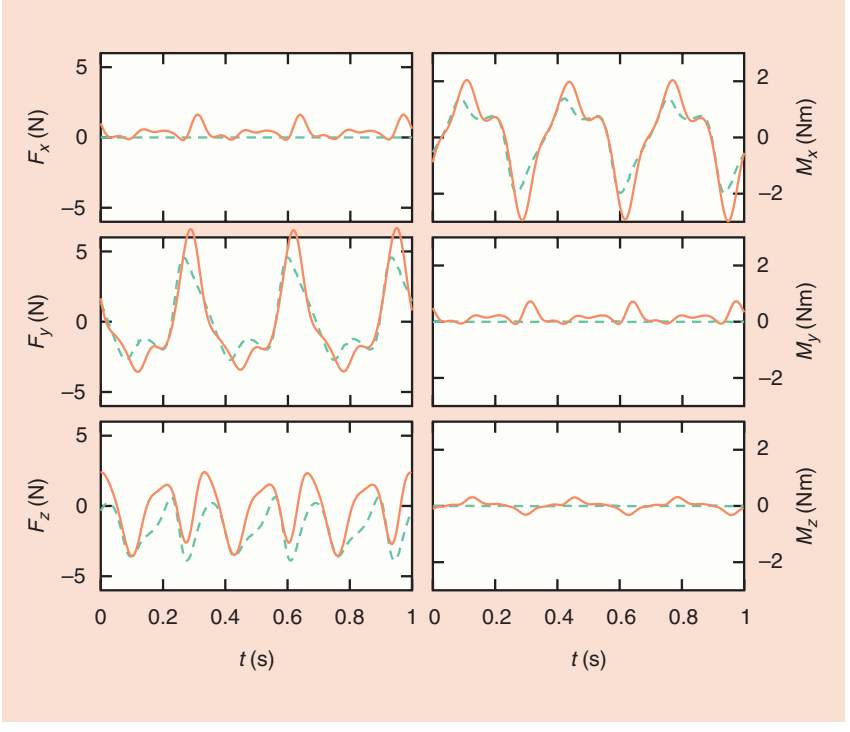

Figure 8. Force measurements in the wind tunnel (solid line), compared to purely inertial forces in a simple two-rigid-body dynamical model (dashed line). Note that F_x is positive on average, implying that the wing generates thrust. $f = 3$ Hz, $\Delta\phi = 5^\circ$, $U_\infty = 0$ ms.

Wind Tunnel Measurements

Exploiting the lateral symmetry of the Robird, a model of half the bird has been placed in a wind tunnel to measure forces on the body and to study the air flow around the beating wing (3 Hz, 5°). The forces are compared to simulation results of a very simple two-rigid-body dynamical model, with the mass distribution of the wing lumped in a front and rear half-wing, both connected to one driving spar. This simple model cannot capture most of the higher-order dynamics or the aerodynamic forces. Figure 8 shows the measured forces, where x points forward (into the tunnel) and z upward (along the wing when upright). The most important experimental observation is in the plot of F_x: The wing generates a positive average thrust force. Figure 7 shows a picture of smoke trail measurements, visualizing the vortices around and behind the wing.

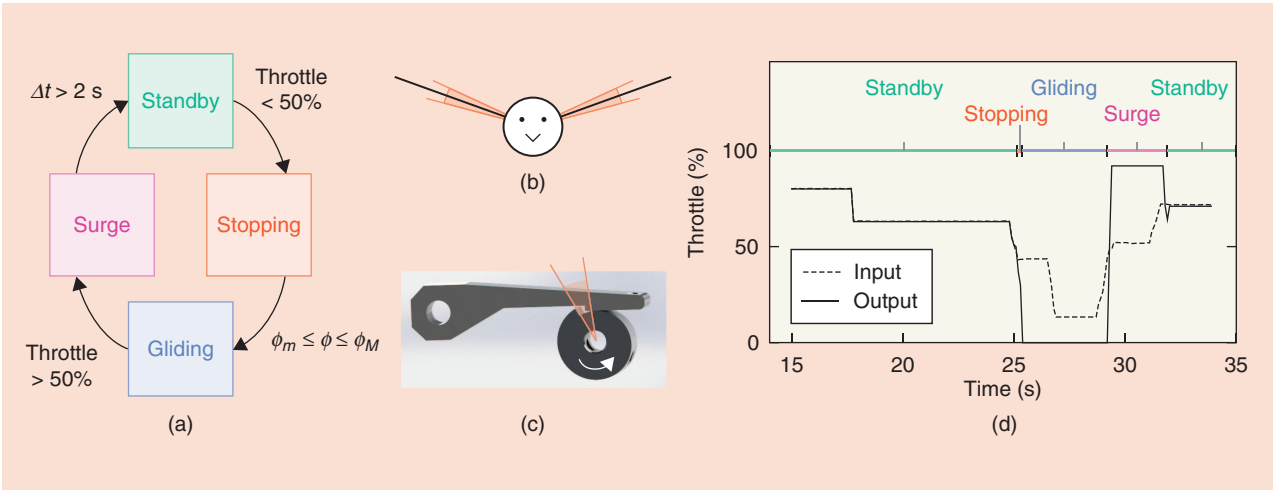

Figure 9. The gliding mode controller automatically engages the mechanism's passive latch when the throttle drops below a threshold. (a) A finite state machine displaying controller states and transition guards. The surge state is required to pull the bird out of gliding mode, by supplying a high throttle for a short time. (b) The range wherein the lift force can engage the gliding lock; the dihedral angle range. (c) The drive shaft/latch range. (d) A demonstration of the gliding controller. The throttle threshold is 50%. The input is the manual RC signal received from the pilot and output goes to the ESC.

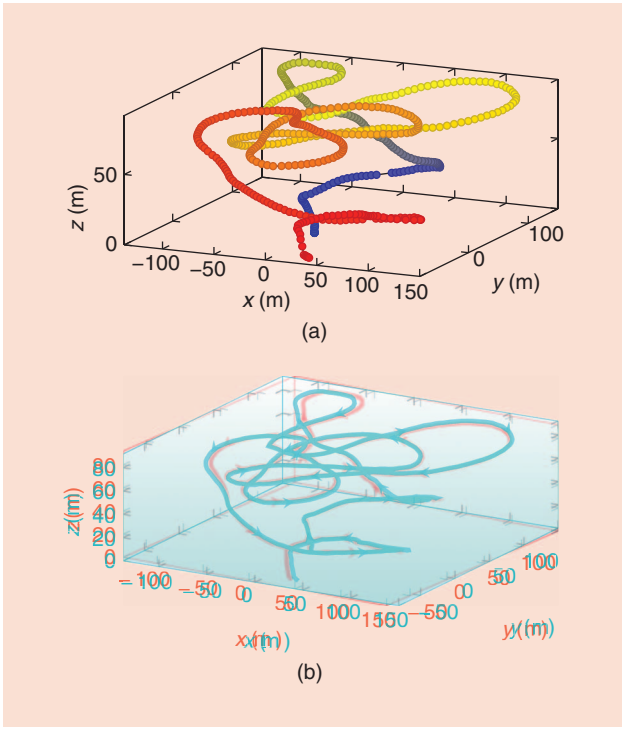

Figure 10. A 3-D flight path log. The bird was brought to altitude in fly-by-wire mode, then autonomously loitered around (0, 0, 80) and (0, 0, 60) [(*x*, *y*, *z*) setpoint in meters] before being brought down to land by the pilot. (a) Flying from blue to red. (b) An anaglyphic 3-D flight path [same as 10(a); view with red/cyan glasses].

Control

Although there are a few very skilled pilots who can manually fly the Robirds, the cognitive load is too extensive when flying close to runways for an entire day. An autopilot system should make flying easier, e.g., in the end, anybody could fly the Robird or program its flight path. When in gliding mode, the bird closely resembles a normal glider plane, and the standard autopilot of the Pixhawk/APM system suffices. The challenge lies in the flapping flight and in switching between modes.

Flight Modes

As shown in the "System" section and Figure 2, the flapping mechanism features a latch that acts as a lock for a passive gliding mode. For the latch to engage—due to the aerodynamic lift pushing the notch wheel backward—the wings must be stopped in the right position, at a dihedral angle of approximately 20° [Figure 9(b)]. A gliding controller takes care of automatically engaging the lock when the throttle drops below a threshold, as depicted in Figure 9. The main drive shaft has an angular encoder measuring the shaft angle ϕ; the latch can engage when $\phi \in [\phi_m, \phi_M]$.

Autopilot

While research on a workable aerodynamic model of the bird in flapping flight is in progress, for stabilizing control, we must rely on existing autopilot controllers offered by the Pixhawk/APM board, tuning parameters by observations of many failed flights, pilot experience, and logged data analysis. We are now at a point where the autopilot can successfully stabilize the system.

There are some challenges left, most of which relate to flapping flight—with vertical accelerations of 3 g in amplitude and heavy pitching, even state estimation is not straightforward. The reason that the autopilot, which was designed for fixed-wing aircraft, only has to be slightly adapted for our flapping-wing system is that the flapping frequency is relatively low compared to smaller-scale ornithopters: 6 Hz is well within the range of the aerodynamics of fixed-wing aircraft, and the autopilot can handle it.

A full path of a flight with the autopilot in stabilizing fly-by-wire mode is shown in Figure 10; the figure eights in the flight path are points when the bird was autonomously loitering.

Conclusion

Some 500 years after his time, Leonardo da Vinci's dreams about artificial flapping-wing flight have come true in ornithopter toys, Robobees, kinematic seagulls, and, now, the Robird. The Robird's similarity to the peregrine falcon allows the spin-off company Clear Flight Solutions [18] to use it for bird control, but, at least equally interesting, are the research opportunities.

There is a qualitative understanding of how flapping-wing flight at this scale works, and simple mechanical and aerodynamical models have been developed. The bird can be controlled in gliding and flapping-wing flight, although the robustness can be improved. Current work, therefore, focuses on improving the dynamic model of the bird, by designing more realistic measurement set-ups and collecting data on both aerodynamic and structural dynamical behavior. From this work, we hope to learn how to improve the flight efficiency and how to conduct proper, on-board state estimation and control on such a highly dynamic system. We also hope to learn whether the principles of the Robird are close to how real birds fly and discover if we could use this system to study real birds.

Acknowledgments

We would like to extend our thanks to Harry Hoeijmakers for initiating research on the Robird, providing valuable comments on the article, and sharing his expertise on the aerodynamics of flapping-wing vehicles. We also thank Cyrano Vaseur and Berend van der Grinten, who have designed, built, and improved the test setup for the aerodynamic studies.

References

[1] L. da Vinci, "*Codice sul volo degli uccelli*," Biblioteca Reale di Torino, 1505.

[2] A. E.-A. S. Soliman Desoky, "A review of bird control methods at airports," *Global J. Sci. Frontier Res.*, vol. 14, no. 2, pp. 41–50, 2014.

[3] V. Battistoni, A. Montemaggiori, and P. Iori, "Beyond falconry between tradition and modernity: a new device for bird strike hazard prevention at airports," in *Proc. Int. Bird Strike Committee, IBSC Meeting and Seminario Internacional Perigo Aviario e Fauna. Brasilia*, 2008, pp. 1–13.

[4] B. Muller, R. Clothier, S. Watkins, A. Fisher. "Design of bio-inspired autonomous aircraft for bird management," in *Proc. 16th Australian Aerospace Congr.*, Melbourne, Australia, 2015, p. 370.

[5] De Persgroep Nederland. (2001, Apr. 11). Vogels op schiphol opgepast voor de 'Horck.' *Trouw*. [Online]. Available: http://www.trouw.nl/tr/nl/4332/Groen/article/detail/1242931/2008/04/11/Vogels-op-Schiphol-opgepast-voor-de-rsquo-Horck-rsquo.dhtml

[6] Festo. (2015, Apr.). Smartbird—bird flight deciphered. [Online]. Available: http://www.festo.com/cms/en_ corp/11369.htm

[7] G. C. H. E. de Croon, K. M. E. de Clercq, R. Ruijsink, B. Remes, and C. de Wagter, "Design, aerodynamics, and vision-based control of the DelFly," *Int. J. Micro Air Vehicles*, vol. 1, no. 2, pp. 71–97, 2009.

[8] R. J. Wood, J. P. Whitney, and B. M. Finio, "Mechanics and actuation for flapping-wing robotic insects," in *Encyclopedia of Aerospace Engineering*, R. Blockley and W. Shyy, Eds. Hoboken, NJ: Wiley, 2010.

[9] J. Ferguson-Lees and D. A. Christie, *Raptors of the World*. Boston, MA: Houghton Mifflin Harcourt, 2001.

[10] L. Meier, D. Honegger, and M. Pollefeys, "PX4: A node-based multithreaded open source robotics framework for deeply embedded platforms," in *Proc. IEEE Int. Conf. Robotics Automation*, 2015, pp. 6235–6240.

[11] J. D. Anderson, *Introduction to Flight*, 7th ed. Boston, MA: McGraw-Hill, 2011.

[12] R. S. Shevell, *Fundamentals of Flight*, 2nd ed. Englewood Cliffs, NJ: Prentice Hall, 1989.

[13] E. Obert, *Aerodynamic Design of Transport Aircraft*. Amsterdam: IOS Press, 2009.

[14] S. Hartman, H. Hoeijmakers, and R. Musters, "Experimental investigation of flow about wing of robot bird," in *Proc. 50th AIAA Aerospace Sciences Meeting Including the New Horizons Forum and Aerospace Exposition*, 2012, pp. 55–63.

[15] H. W. Hoeijmakers and J. Mulder, "Computational and experimental investigation into flapping wing propulsion," in *Proc. 54th AIAA Aerospace Sciences Meeting*, 2016, pp. 802–834.

[16] G. Taylor, R. Nudds, and A. Thomas, "Flying and swimming animals cruise at a Strouhal number tuned for high power efficiency," *Nature*, vol. 425, pp. 707–711, Oct. 2003.

[17] M. F. Platzer, K. D. Jones, J. Young, and J. C. S. Lai, "Flapping-wing aerodynamics: Progress and challenges," *AIAA J.*, vol. 46, no. 9, pp. 2136–2149, 2008.

[18] Clear Flight Solutions. (2016). Robotic bird control. [Online]. Available: http://clearflightsolutions.com

Gerrit Adriaan Folkertsma, Robotics and Mechatronics Group, Center for Telematics and Information Technology Institute, University of Twente, Enschede, The Netherlands. E-mail: g.a.folkertsma@ieee.org.

Wessel Straatman, Clear Flight Solutions, Enschede, The Netherlands. E-mail: w.straatman@clearflightsolutions.com.

Nico Nijenhuis, Clear Flight Solutions, Enschede, The Netherlands. E-mail: nijenhuis.nico@gmail.com.

Cornelis Henricus Venner, Department of Engineering Fluid Dynamics, Faculty of Engineering Technology, University of Twente, Enschede, The Netherlands. E-mail: c.h.venner@utwente.nl.

Stefano Stramigioli, Robotics and Mechatronics Group, Center for Telematics and Information Technology Institute, University of Twente, Enschede, The Netherlands. E-mail: S.Stramigioli@ieee.org.